PNAS RESEARCH ARTICLE | EARTH, ATMOSPHERIC, AND PLANETARY SCIENCES OPEN ACCESS

Garnet secondary ion mass spectrometry oxygen isotopes reveal crucial roles of pulsed magmatic fluid and its mixing with meteoric water in lode gold genesis

Gao-Hua Fan[a,b], Jian-Wei Li[a,b,1], John W. Valley[c], Maria Rosa Scicchitano[c,d], Philip E. Brown[c], Jin-Hui Yang[e], Paul T. Robinson[a,b], Xiao-Dong Deng[a], Ya-Fei Wu[a,b], Zhan-Ke Li[a,b], Wen-Sheng Gao[b], Si-Yuan Li[b], and Shao-Rui Zhao[b]

Edited by Bruce Watson, Rensselaer Polytechnic Institute, Troy, NY; received September 6, 2021; accepted March 15, 2022

Lode gold deposits, which are currently the world's major gold supply, have been shown to be generated mostly by phase separation of metamorphic fluids and/or interaction between these fluids and wall rocks. Here we use garnet oxygen isotopes by secondary ion mass spectrometry to document the crucial role of magmatic hydrothermal fluids and their mixing with meteoric water in the formation of the world-class Dongping gold deposit in the North China Craton. Garnet grains from quartz veins of various paragenetic stages and the mineralized alteration envelope at Dongping have dynamic $\delta^{18}O$ variations of 3.8 to −11.0‰, with large intragrain fluctuations up to 5.3‰. These values correspond to calculated $\delta^{18}O$ values of 6.1 to −9.1‰ for the hydrothermal fluids from which the garnet formed. The isotope data, notably the cyclic alternation in $\delta^{18}O$ within individual garnet grains, are best interpreted to reflect multiple pulses of magmatically derived fluids and subsequent mixing of each pulse with variable amounts of meteoric water. The results presented here allow us to quantify the significant interplay between magmatic hydrothermal fluids and meteoric water that spanned the entire mineralization history and triggered gold deposition of a lode gold deposit. This study highlights the potential use of in situ oxygen isotope analysis of garnet in tracing the origin and evolution of hydrothermal fluids in the Earth's crust that may have formed other giant ore deposits.

garnet | oxygen isotope | magmatic fluid | meteoric water | lode gold deposit

Lode gold deposits, which account for one-third of the world's gold resources and typically consist of structurally controlled quartz-sulfide veins and sulfide disseminations in hydrothermally altered wall rocks, have been formed in a variety of geodynamic environments. These deposits are widely distributed in cratonic blocks and orogenic belts and range in age from Archean to Cenozoic (1, 2). It is commonly thought that most lode gold deposits, particularly those in Phanerozoic orogenic belts, precipitated mostly from metamorphic fluids generated by the devolatilization of fertile sedimentary and volcanic rocks during accretionary or collisional orogenesis (2–6). Some studies, however, argue for an important role of magmatic hydrothermal fluids in the formation of this type of deposit (7–11). Previous constraints on fluid source of lode gold deposits have been based mainly on bulk-sample analyses of stable isotopes (C, H, O, S, and N) of ore and gangue minerals, chiefly pyrite, quartz, sericite, calcite, and ankerite (7, 9, 11). Unfortunately, bulk-sample analyses may represent averages of multiple generations of minerals precipitated from different fluids or from a single evolving fluid that was repeatedly modified isotopically. In either case, the averaged isotopic compositions can be problematic when used to fingerprint the source and/or evolution of the ore-forming fluids. As such, the question of whether or not magmatically dominated fluids have played a critically important role in lode gold genesis remains unresolved. Another important issue in the study of lode gold deposits is the mechanisms responsible for gold deposition. Precipitation of gold in lode deposits is commonly attributed to depressurization and boiling of fluids and/or fluid–rock interaction (2, 6, 12–14). With regard to fluid mixing between the ore fluid and an external component (commonly meteoric water), the prevalent viewpoint is that this process, if any, occurs merely in the late stage of mineralization and thus makes little or no contribution to gold deposition (2, 5, 6, 13, 14).

To address these problems, we focused on the in situ oxygen isotopic compositions of garnet, a not uncommon hydrothermal mineral in many lode gold deposits worldwide. Garnet is typically characterized by extremely slow intragrain diffusion of oxygen isotopes, even at magmatic temperatures (850 to 900 °C) (15, 16) that are significantly higher than the formation temperatures of hydrothermal ore deposits, thereby allowing

Significance

There is a common consensus that lode gold deposits mostly precipitated from metamorphic fluids via fluid boiling and/or fluid–rock interaction, but whether magmatic hydrothermal fluids and the mixing of such fluids with an external component have played a vital role in the formation of lode gold deposits remains elusive. We use garnet secondary ion mass spectrometry oxygen isotope analysis to demonstrate that the world-class Dongping lode gold deposit has been formed by multiple pulses of magmatic hydrothermal fluids and their mixing with large volumes of meteoric water. This study opens an opportunity to tightly constrain the origin of lode gold deposits worldwide and other hydrothermal systems that may have generated giant ore deposits in the Earth's crust.

Author contributions: G.-H.F. and J.-W.L. designed research; G.-H.F., J.-W.L., J.W.V., M.R.S., and P.E.B. performed research; J.W.V., M.R.S., and P.E.B. contributed new reagents/analytic tools; G.-H.F., J.-W.L., J.W.V., M.R.S., P.E.B., J.-H.Y., P.T.R., X.-D.D., Y.-F.W., Z.-K.L., W.-S.G., S.-Y.L., and S.-R.Z. analyzed data; G.-H.F. and J.-W.L. wrote the paper; G.-H.F., J.-W.L., W.-S.G., and S.-Y.L. contributed field investigation and sample collection; J.W.V., M.R.S., and P.E.B. contributed manuscript editing and data interpretation; J.-H.Y., P.T.R., and Y.-F.W. contributed manuscript editing; X.-D.D. contributed manuscript editing and sample preparation; Z.-K.L. performed electron probe microanalysis and laser ablation inductively coupled plasma mass spectrometry analysis; and S.-R.Z. performed scanning electron microscopy and electron probe microanalysis.

The authors declare no competing interest.

This article is a PNAS Direct Submission.

Copyright © 2022 the Author(s). Published by PNAS. This open access article is distributed under Creative Commons Attribution-NonCommercial-NoDerivatives License 4.0 (CC BY-NC-ND).

[1]To whom correspondence may be addressed. Email: jwli@cug.edu.cn.

This article contains supporting information online at http://www.pnas.org/lookup/suppl/doi:10.1073/pnas.2116380119/-/DCSupplemental.

Published May 2, 2022.

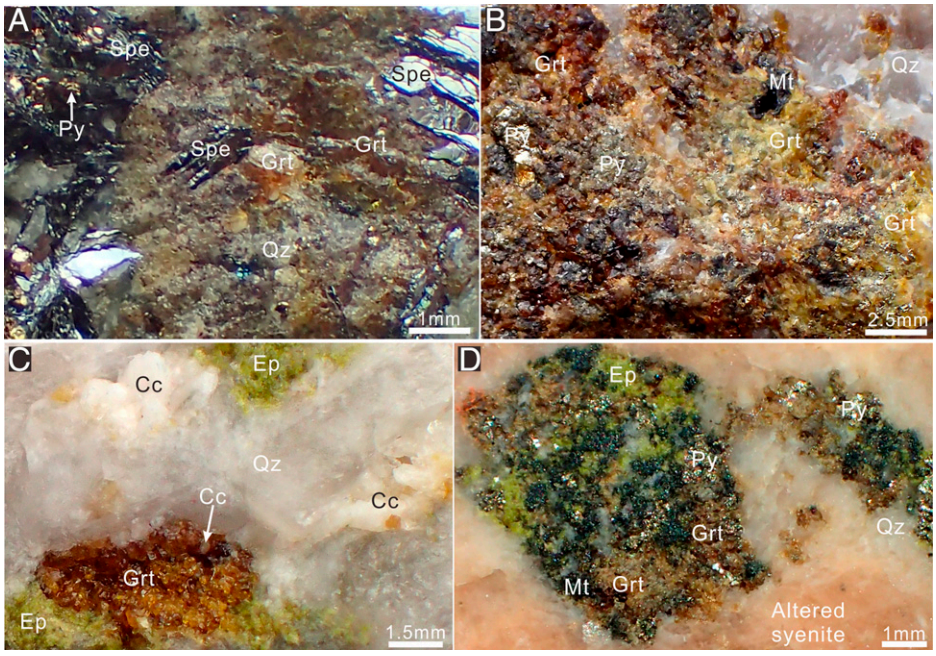

Fig. 1. Photographs showing three garnet-bearing vein samples (*A*–*C*) and a mineralized alteration envelope (*D*) used for this study. (*A*) Preore quartz-specularite vein containing abundant brown garnet grains. (*B*) Massive aggregates of brown and beige garnet associated with auriferous pyrite and magnetite in a syn-ore quartz vein. (*C*) Brown garnet coexisting with epidote and calcite as cavity infillings in a postore quartz vein. (*D*) Brown garnet intergrown with pyrite, magnetite, and epidote in mineralized alteration envelope. Grt, garnet; Py, pyrite; Qz, quartz; Spe, specularite; Mt, magnetite; Cc, calcite; Ep, epidote.

the garnet to retain its original oxygen isotopic signature. Thus, garnet can be an ideal, robust recorder of oxygen isotopic compositions of fluid and melt from which the mineral crystallized. Here, we present oxygen isotope results by secondary ion mass spectrometry (SIMS) for garnet from the world-class Dongping gold deposit in the North China Craton and use these data to shed light on the source and subtle evolution of the ore-forming fluids. The results reveal repeated injections of magmatically derived fluid pulses and subsequent mixing of individual pulses with meteoric water throughout the entire ore-forming process. The role of such fluid mixing in triggering gold precipitation is also discussed.

Results

Deposit and Sample Descriptions. The Dongping gold deposit (~120 t Au) in the Zhang-Xuan district of the North China Craton is one of several dozen large lode gold deposits in this craton. It is hosted in the Devonian Shuiquangou alkaline complex (*SI Appendix*, Fig. S1), which consists of syenite and minor monzonite. The complex intrudes amphibolite- to granulite-facies rocks of the Neoarchean Sanggan Group (2,715 ± 21 Ma) (17) and has a zircon U-Pb age of 392 ± 2 Ma (18). Gold mineralization consists of fault-controlled, high-grade quartz-sulfide veins (3 to 30 g/t Au but locally up to 300 g/t) and low-grade disseminated ores in alteration envelopes (<5 g/t Au). On the basis of field relations and petrographic data, three paragenetic stages are well established: 1) a preore stage marked by K-feldspar-quartz-specularite veins; 2) a syn-ore stage largely manifested by quartz-sulfide-magnetite veins and sulfide-magnetite disseminations in alteration envelopes surrounding auriferous quartz veins; and 3) a postore stage represented by barren quartz-calcite veins (18). Abundant tellurides are present in the syn-ore quartz veins and are sporadically observed in disseminated ores, showing a close association with native gold in both mineralization styles. Notably, hydrothermal garnet grains occur in quartz veins of all three paragenetic stages and the mineralized alteration envelopes. The garnet grains yielded U-Pb ages of 142 ± 5 to 139 ± 6 Ma, which are interpreted as the age of gold mineralization at Dongping (18).

A total of 17 garnet grains from four samples were selected for this study, including three vein samples, one each from the pre-, syn-, and postore stages and one from the mineralized alteration envelope (Fig. 1). Mineralogical characters and textural features for the samples are summarized in Dataset S1. Garnet grains from the syn-ore vein (~100 g/t Au) range in color from brown to beige, whereas those from the pre- and postore veins and the mineralized alteration envelope are generally brown (Fig. 1).

Textures and Geochemical Compositions of the Garnet. The internal textures of all garnet grains were investigated using scanning electron microscopy (SEM). Most grains are characterized by well-developed oscillatory zoning and locally show resorption or dissolution textures in the cores, rims, or intermediate zones (Fig. 2 and *SI Appendix*, Fig. S2). Irregular wavy growth zones are also developed in some grains (e.g., grain G13; Fig. 2), which are commonly interpreted to reflect changes in pressure of garnet-forming fluids (19). It is noteworthy that the syn-ore garnet grains are closely associated with auriferous magnetite and pyrite (e.g., grains G6, G7, and G8; *SI Appendix*, Fig. S2).

Major oxide and trace element compositions of each grain were determined using electron probe microanalysis (EPMA) and laser ablation inductively coupled plasma mass spectrometry (LA-ICP-MS), respectively. Garnet grains from preore veins and the mineralized alteration envelope are predominantly andradite with variable amounts of grossularite ($Adr_{100–56}$ $Grs_{0–41}$), whereas those from syn- and postore veins show a relatively larger variation in composition ($Adr_{100–26}Grs_{0–66}$; Fig. 2, *SI Appendix*, Fig. S3, and Dataset S2). The rare earth element (REE) contents of garnet grains from each paragenetic stage are highly variable, ranging from 488 to 0.1 μg/g (Fig. 2, *SI Appendix*, Fig. S4, and Dataset S3).

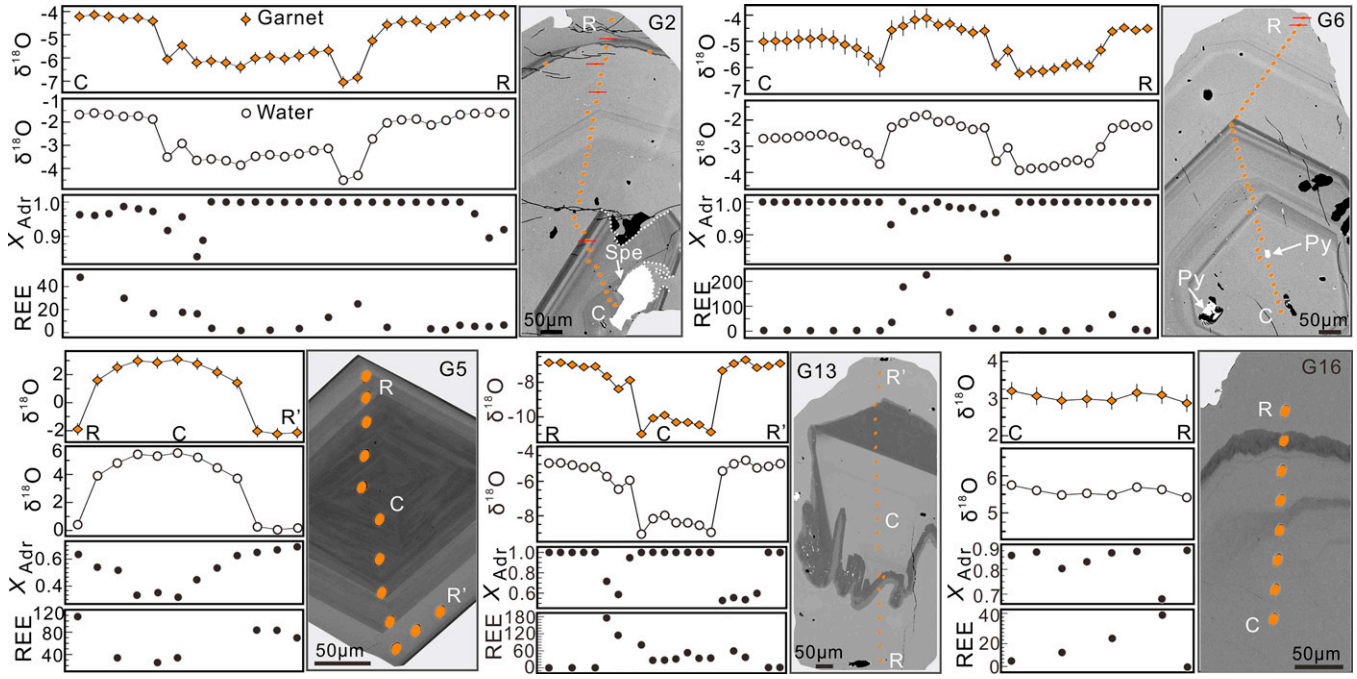

Fig. 2. Values of and variations in $\delta^{18}O$ (‰) of representative garnet grains from pre- (grain G2), syn- (grains G5; G6), and postore (grain G13) veins and mineralized alteration envelope (grain G16). Also shown are the calculated $\delta^{18}O_{water}$ values in per mille, X_{Adr} values, and total REE contents in micrograms per gram. Back-scattered electron images showing the zoning textures of garnet grains. Ellipses in garnet grains show areas of SIMS spot analysis. Red lines within grains G2 and G6 represent spot analyses that were discarded because no major compositions were analyzed for those areas and thus cation matrix correction was not applicable. White dashed-dotted lines in grain G2 show the resorption and/or dissolution texture. Note that oxygen isotope ratios fluctuate along core to rim traverses. Error bars are ±2SD. C, core; R/R′, rim; Spe, specularite; Py, pyrite.

The oxygen isotopic ratios of garnet grains analyzed using SIMS have a repeatability better than ±0.3‰ (2SD) and an estimated accuracy of ±0.5 to 0.6‰ [2SD (16)]. Values of $\delta^{18}O$ for garnet ($\delta^{18}O_{garnet}$) and the calculated values for water in equilibrium with garnet ($\delta^{18}O_{water}$) are summarized in Dataset S4 and graphically illustrated in Figs. 2 and 3 and *SI Appendix*, Fig. S5. Garnet grains from all three vein samples show large variations in $\delta^{18}O$, ranging from 2.8 to −7.0‰ in preore garnet, from 3.1 to −11.4‰ in syn-ore garnet, and from −4.1 to −11.0‰ in postore garnet. Three brown grains from the mineralized alteration envelope have relatively higher and more restricted $\delta^{18}O$ values of 3.8 to 0.5‰. Systematic analyses along most grain traverses reveal dynamic fluctuations in $\delta^{18}O$ values, showing rim-ward decreases or increases (e.g., grain G5; Fig. 2) or cyclical alternations over the entire grain (e.g., grains G2 and G6; Fig. 2). The largest and smallest intragrain $\delta^{18}O$ variations are observed in two syn-ore brown garnet grains, which are 3.1 to −2.2‰ for grain G5 and 3.2 to 2.9‰ for grain G16 (Fig. 2). The syn-ore beige garnet grains generally have much lower $\delta^{18}O$ values than coexisting brown grains, with the lowest value of −11.4‰ in grain G10 (Fig. 3). Based on the garnet formation temperatures determined by fluid inclusion microthermometry in the three paragenetic stages [383 to 302 °C (18)] and the oxygen isotope fractionation equations for andradite-water and grossular-water (20), $\delta^{18}O_{water}$ values were calculated to be 5.3 to −4.5‰ for preore vein, 5.5 to −9.1‰ for syn-ore vein, −2.2 to −9.1‰ for postore vein, and 6.1 to 3.1‰ for the mineralized alteration envelope (Fig. 3).

Discussion

A Magmatic Origin of the Ore Fluids. Dongping garnet formed at the temperature range of 383 to 302 °C (18), under which oxygen diffusion in garnet can be neglected (15, 16). Thus, the measured $\delta^{18}O$ values represent the original oxygen isotopic compositions of garnet, suggesting that the calculated $\delta^{18}O_{water}$ values can be reliably used to decipher fluid source and evolution. The calculated $\delta^{18}O_{water}$ values for pre- and syn-ore veins are up to 5.3‰ and 5.5‰, respectively, and attain 6.1‰ for the mineralized alteration envelope (Fig. 3). They are consistent with values of most magmatic hydrothermal Au–Cu deposits worldwide [$\delta^{18}O_{water}$ = 5 to 10‰ (21, 22)] but lower than the typical range of ore fluids related to the world's Phanerozoic orogenic lode gold deposits that were generated by metamorphic devolatilization of sedimentary rocks [$\delta^{18}O_{water}$ = 7 to 15‰ (2, 12, 23)]. Gold mineralization at Dongping postdated the amphibolite- to granulite-facies rocks of the Neoarchean Sanggan Group at least by 2.5 Gy (17, 18), precluding the possibility that the ore fluids were derived from metamorphic dewatering of those rocks. We therefore favor a magmatic origin for the ore fluids in the Dongping gold deposit. This view is further supported by the ubiquitous presence of abundant tellurides at Dongping (18), a feature that has been widely cited as a diagnostic indicator for a magmatic fluid source of many hydrothermal ore systems (14, 24). However, the magmatic hydrothermal fluid at Dongping is unlikely to have been derived from the Devonian ore-hosting Shuiquangou alkaline complex as previously thought (17), because U-Pb dating of the garnet shows that gold mineralization occurred at 142 ± 5 to 139 ± 6 Ma (18). Rather, the ore fluids were most likely sourced from degassing of an underlying magma chamber, presumably represented by the Early Cretaceous Shangshuiquan granite [U-Pb age of 143 ± 1 Ma (18)] immediately to the southeast of the Dongping gold deposit (*SI Appendix*, Fig. S1).

Although contact metamorphism induced by intrusion of deep-seated magmas may have led to devolatilization of the country rocks and thus contributed to ore-related fluids, this scenario is less likely for the Dongping gold deposit. The

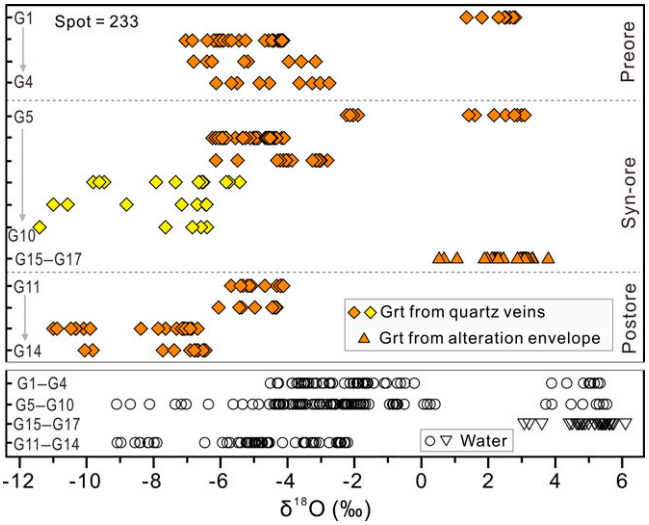

Fig. 3. $\delta^{18}O$ values (per mille) of garnet grains and equilibrated fluid for pre- (grains G1 to G4), syn- (grains G5 to G10), and postore (grains G11 to G14) vein stages and mineralized alteration envelope (grains G15 to G17). Brown diamonds and triangles represent brown grains in various veins and alteration envelope, respectively, whereas yellow diamonds represent beige garnet grains (grains G8 to G10). Each row corresponds to data obtained from a single garnet grain with an exception of grains G15 to G17 that plot in the same row because of their relatively restricted $\delta^{18}O$ values. Calculated $\delta^{18}O_{water}$ values for each stage are grouped together and shown in separate rows. Note that the serial numbers for single garnet grains at the same stage do not indicate the chronologic order of garnet crystallization.

amphibolite-facies rocks of the Sanggan Group have undergone significant devolatilization and granulites therein are nearly anhydrous, and thus few fluids were available to be released during subsequent contact metamorphism. Moreover, those rocks were successively intruded by voluminous magmas as represented by the Paleoproterozoic granite, the Devonian alkaline complex, and the Triassic granite in the Zhang-Xuan district, with a combined exposure of >500 km^2 (18). Such voluminous magmatism would likely have caused contact metamorphism of the amphibolite-facies rocks and further liberated volatiles from the rocks. Consequently, there would be very few fluids remaining to be released from those highly devolatilized rocks during the Early Cretaceous magmatic episode. It is also unlikely that ore fluids were mainly derived from metamorphic devolatilization of the ore-hosting alkaline complex, because local mapping and drill core logging of >700 m have revealed no signs of extensive contact metamorphism (18). Based on the maximum gold concentrations (0.016 μg/g) in modern gold-rich systems (25), >7 × 10^6 m^3 gold-bearing fluids are required to form the giant Dongping deposit with reserves of 120 t Au. Such large voluminous fluids are unlikely to have been produced by contact metamorphism of the ore-hosting alkaline complex induced by the underlying, ore-related magma chamber. Rather, such large fluid fluxes can be best interpreted in terms of degassing of a deep-seated magma chamber (26).

Incursion of Meteoric Water. Various garnet grains of the same stage and different growth zones within single grains show large variations in $\delta^{18}O_{garnet}$ values with different mole fractions of andradite ($\delta^{18}O$ = 3.8‰ with X_{Adr} of 0.58 and $\delta^{18}O$ = −11.4‰ with X_{Adr} of 0.99; *SI Appendix*, Fig. S3). These isotopic variations (3.8 to −11.4‰) cannot be explained by octahedral cation substitution (Fe, Al) within garnet, because such a crystallographic factor has little effect on $\delta^{18}O$ fractionation between andradite and grossular [$\Delta^{18}O_{Adr\text{-}Grs}$ <0.8‰ (19, 27)]. Similarly, temperature changes cannot account for the intra- or intercrystalline differences in the calculated $\delta^{18}O_{water}$ values (Fig. 2 and *SI Appendix*, Fig. S5), as the range of formation temperatures of Dongping garnet [383 to 302 °C (18)] can only explain a $\delta^{18}O_{water}$ shift lower than 0.7‰ (19). The $\delta^{18}O$ fractionation of fluid may also be caused by phase separation due to the salt effect of NaCl (28), but salinity differences (<9 wt. % NaCl equiv.) between liquid- and vapor-rich inclusions in Dongping garnet, which were generated by fluid immiscibility (18), could only account for up to 0.45‰ difference in $\Delta^{18}O_{fluid\text{-}garnet}$ (28, 29). Interaction between magmatic hydrothermal fluid [$\delta^{18}O_{water}$ = 5 to 10‰ (21, 22)] and the ore-hosting syenite [average $\delta^{18}O$ = 7.1‰ (30)] may have modified oxygen isotopic compositions of the resultant fluids. Numerical modeling shows that, in both closed and open systems at the garnet-forming temperatures (300 to 400 °C), the minimum $\delta^{18}O$ value of the resultant fluids is 2.2‰ (*SI Appendix*, Fig. S6 *A* and *B*), which is inconsistent with the predominance of negative $\delta^{18}O_{water}$ values at Dongping (Fig. 3). We therefore preclude the possibility that the large spread in $\delta^{18}O_{garnet}$ values at Dongping was caused by the aforementioned fluid–rock interaction. The lack of a progressive elevation in $\delta^{18}O_{garnet}$ from core to rim along most grain traverses further argues against such a reaction scenario.

In lode gold systems, an external fluid, most commonly meteoric water, can percolate into the upper crust and reach the depth of ore precipitation (12). Fluid inclusions contained in calcite from the postore stage of Dongping and another medium-sized gold deposit in close proximity to Dongping, both forming at *ca.* 140 Ma (18, 31), have δD of −84.4 to −97.0‰ (30, 31). These values have been considered to approximate hydrogen isotopes of local meteoric water that was involved during mineralization of those two deposits (30, 31). The $\delta^{18}O$ values of that meteoric water are calculated at −13.3 to −11.8‰ (average = −12.5‰) according to the meteoric water line in the δD versus $\delta^{18}O$ diagram (32). If isotopic exchange between such meteoric water and the host syenite is the case for Dongping, the resultant fluids would have $\delta^{18}O$ values not higher than 4.5‰ even at an extremely low water/rock ratio (*SI Appendix*, Fig. S6*C*). Such a low water/rock ratio is very unlikely given that the veins investigated are all hosted in and structurally controlled by brittle faults (18). Garnet grains from each vein stage have negative $\delta^{18}O$ values as low as −11.4‰ (Fig. 3) and such low $\delta^{18}O_{garnet}$ values can only be produced by significant influxes of externally derived, low-$\delta^{18}O$ meteoric water in the ore-related magmatic hydrothermal system.

Previous studies have shown that a decrease in X_{Adr} values and REE contents of garnet reflects influxes of meteoric water (33–35). At Dongping, however, those two parameters show variable (positive, negative, and weak) correlations with $\delta^{18}O_{garnet}$ values (Fig. 2 and *SI Appendix*, Figs. S3 and S4), implying that X_{Adr} values and REE contents of garnet are not always reliable when used as indicators for the involvement of meteoric water in hydrothermal systems. Fluctuations in Fe and Al contents as shown by oscillatory and wavy growth zones in garnet (Fig. 2 and *SI Appendix*, Fig. S2) have been linked to varying growth rates that in turn control the incorporation of REE into garnet via coupled substitution in Fe and Al sites (19). Moreover, precipitation of various minerals (e.g., iron oxide, epidote, and sulfide; Fig. 1) could have consumed Fe, Al, and REE, leading to depletions of those elements in the residual hydrothermal fluids and consequently in garnet crystallized from the fluids. As a result, the variations in X_{Adr} values and REE contents in garnet may not necessarily reflect

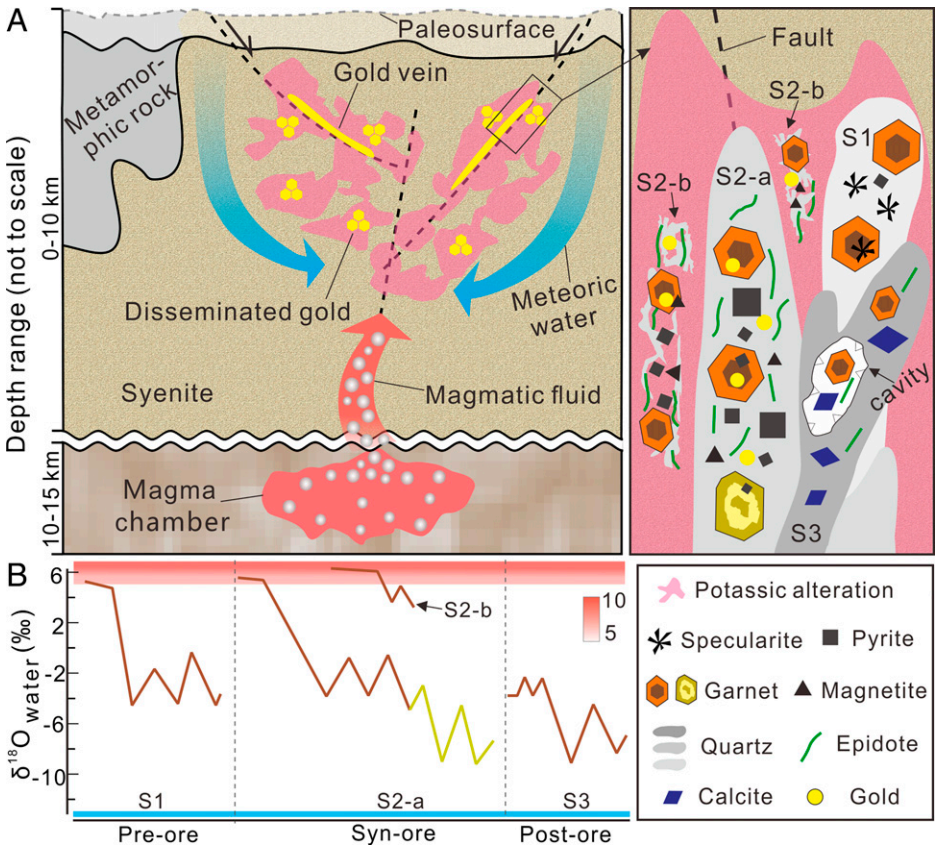

Fig. 4. A schematic illustration showing the hydrothermal fluid system from which various minerals precipitated to form the Dongping gold deposit. (*A*) Magmatic fluid pulses were repeatedly exsolved from the underlying magma chamber. Faults and fractures as conduits facilitated ascending of magmatically derived fluids and subsequently their mixing with voluminous meteoric water, processes leading to gold deposition and associated veining, whereas the disseminated mineralization in alteration envelopes occurred in less-fractured wall rocks where the infiltration of meteoric water is less conspicuous. Various mineral assemblages in pre- (S1), syn- (S2-a), and postore (S3) veins and the mineralized alteration envelopes (S2-b) formed in response to variable fluid mixing. (*B*) Evolution trend of $\delta^{18}O_{water}$ values of garnet grains from each paragenetic stage indicating pulsed influxes of magmatic fluids [red bar; $\delta^{18}O_{water}$ = 5 to 10‰; (21, 22)] and incursions of meteoric water [blue bar; average $\delta^{18}O_{water}$ = −12.5‰; (30, 31)]. The range and variations of oxygen isotopic ratios for each stage are defined using $\delta^{18}O_{water}$ values shown in Fig. 3 and *SI Appendix*, Fig. S5. The brown and beige solid lines correspond to the brown and beige garnet grains, respectively.

incursion of meteoric water. Taking all the information together, we propose that the dynamic and significant variations both in $\delta^{18}O_{garnet}$ and $\delta^{18}O_{water}$ values can be best interpreted in terms of repeated mixing between individual pulses of magmatically derived fluids from an underlying magma chamber and low-$\delta^{18}O$ meteoric water.

Hydrothermal Fluid System Associated with Lode Gold Genesis. Repeated influxes of magmatic fluids isotopically revealed by Dongping garnet grains are most likely related to episodic fluid exsolution from the deep-seated crustal magma chamber and/or complicated fracturing. This view, in turn, indicates thermal stability of the underlying magma chamber, which either reflects slow cooling of a large-volume magma chamber (36) or multiple injections of new batches of mafic magma into the chamber (37). When silicate melts in the magma chamber reached volatile saturation, ore fluids were released and ascended along brittle fault systems as represented by abundant thick quartz veins at Dongping (*SI Appendix*, Fig. S1). Subsequently, mixing of magmatically derived fluids with convecting meteoric water led to the deposition of gold ores and associated mineral assemblages (Fig. 4*A*).

At Dongping, a few brown garnet grains in the pre- and syn-ore veins were precipitated initially from magmatically dominated fluids, followed by rim growth in response to the incursion of more meteoric water. Other brown grains in the same veins formed as a result of continuous mixing between new pulses of magmatic hydrothermal fluids and varying amounts of meteoric water (Fig. 4*B*). The greatest input of meteoric water into the magmatic hydrothermal system are recorded in syn-ore beige garnet and postore brown varieties (Fig. 4*B*). Based on isotopic mass balance calculations for binary mixing, the input percentage of meteoric water at the various veining stages is estimated to range from 85 to 3% (mainly between 71 and 34%; Dataset S5). The large extent of mixing between magmatic and meteoric fluids resulted from mechanically enhanced permeability along vein fracture zones, which allowed infiltration of voluminous meteoric water into the magmatically derived fluid system (Fig. 4*A*). We note that low influxes of meteoric water (<32%; Dataset S5) took place mainly during formation of the alteration envelopes as recorded in much higher $\delta^{18}O$ values of the garnet grains therein (Figs. 3 and 4*B*). This observation is consistent with the lower permeability of the wall rocks compared to that of the fracture zones in which the veins were deposited (Fig. 4*A*). Collectively, our study documents that meteoric water has played an important role in the hydrothermal fluid system of both pre- and syn-ore stages at Dongping (Fig. 4*B*), in sharp contrast to existing models for most lode gold deposits that predict the input of meteoric water only in the postore stage and thus has no direct relationship with gold deposition (2, 3, 5, 6).

The solubility of gold in hydrothermal fluids of lode deposits is dominated by $Au(HS)_2^-$ complexing (12), which in turn is controlled by the temperature, pressure, acidity and redox state of the fluids (38, 39). Changes in various combinations of these factors can effectively trigger gold deposition (38, 39). The syn-ore garnet grains at Dongping record frequent incursions of meteoric water into the magmatic fluids. Such a process would have lowered the temperature and elevated both the pH and oxygen fugacity of hydrothermal system, thus destabilizing gold bisulfide complexes (38, 39) and causing gold deposition. This view is supported by the close relationship between the low-$\delta^{18}O$ growth zones of syn-ore garnet and the auriferous magnetite and pyrite that usually contain inclusions of native gold (*SI Appendix*, Fig. S2 and ref. 18). The lack of gold mineralization in the preore stage is presumably due to the low budget of reduced sulfur in the early-stage magmatic fluids, as indicated by the common occurrence of specularite and the scarcity of sulfide minerals (Fig. 1*A*), thus preventing the gold from being complexed and transported by reduced sulfur from the magma chamber. The barren, postore veins may have been formed from metal-deficient fluids derived from highly evolved melts in the magma chamber.

Implications for Tracing Ore-Fluid Source of Lode Gold Deposits. The source of ore-forming fluids is of critical importance for a better understanding of the genesis of lode gold deposits and thus has attracted much attention in the study of this very important type of gold deposit. A longstanding debate exists whether or not magmatically derived fluids have played an important role in the formation of lode gold deposits (5, 6). Source of mineralizing fluids in the Dongping gold deposit has been extensively studied mainly by oxygen isotope analysis of bulk quartz separates and hydrogen isotope analysis of fluid inclusions in the quartz, with the bulk δD and $\delta^{18}O_{water}$ values plotting marginally to the magmatic fluid field in the δD-$\delta^{18}O$ diagram and, more commonly, in an area intermediate between that field and meteoric water line (40). These isotope data have been interpreted as indicating magmatic derivation of the ore fluids and introduction of meteoric water in the hydrothermal system during postore stage (40). The present results of garnet SIMS oxygen isotope analysis suggest that previous bulk δD and $\delta^{18}O$ data represent mixtures of multiple pulses of magmatically derived fluids and variable amounts of meteoric water, and thus are problematic or less precise when used to track the source and evolution of ore fluids. Our study shows that a single garnet grain may consist of multiple and/or complex growth zones that record dynamic isotopic variations due to repeated interplays between different end-member fluids. As such, in situ $\delta^{18}O$ analysis, combined with textural characterization of garnet, can provide a more robust approach to fingerprint the origin and subtle evolution of ore fluids of lode gold deposits. In cases where garnet is lacking in such deposits, in situ $\delta^{18}O$ analysis of quartz can be a promising complementary or an alternative approach, because quartz is the most common mineral spanning the whole history of lode gold genesis and typically displays complicated textures (41) that bear a wealth of information on the source, nature, and evolution of gold mineralizing fluids. With increasing utilization of in situ analytical techniques for the measurement of $\delta^{18}O$, the existing bulk $\delta^{18}O$ data for many lode gold deposits worldwide and their geological significance could be revisited. Consequently, it is expected that the crucial role of magmatically derived fluids and their mixing with meteoric water may be increasingly recognized in lode gold genesis.

Conclusion

Our systematic SIMS oxygen isotope study of zoned garnet grains provides significant insights into the source and subtle evolution of the ore-forming fluids in the Dongping gold deposit. Highly variable $\delta^{18}O$ values of the garnet reveal multiple pulses of magmatically derived fluids that individually mixed with a large volume of meteoric water throughout the history of gold mineralization. The results of this study, which highlights the crucial role of magmatic hydrothermal fluids and their mixing with meteoric water in lode gold deposition, stand in stark contrast to the most commonly held model for lode gold deposits. Our data also show that the X_{Adr} values and REE contents of garnet are variably related to fluid source, growth kinetics, and/or changes in fluid chemistry associated with precipitation of other minerals. As such, great caution should be taken when X_{Adr} values and REE contents of garnet are used as fingerprints for fluid source. A far-reaching implication of this study is that in situ $\delta^{18}O$ values of well-characterized garnet and other minerals (e.g., quartz) can significantly advance our understanding of the source and evolution of hydrothermal systems in Earth's crust from which a large variety of ore deposits have been formed.

Methods

Sample Preparation. Most garnet grains were hand-picked under a binocular microscope after crushing and the remaining grains were drilled from double-polished thin sections. These garnet grains were then cleaned in an ultrasonic bath with distilled water and mounted within 5 mm of center of 25-mm epoxy disks, with the UWG-2 garnet reference material (42) in the center of the mount. Each mount was then polished to expose grain interiors. An optical microscope and a white-light profilometer were used to monitor scratches and polishing relief and to ensure a flat surface.

SEM and EPMA. All garnet grains were imaged using optical microscopy and SEM to reveal growth zones and possible presence of any mineral inclusions, which were used as landmarks for subsequent SIMS analysis. Back-scattered electron imaging was used to characterize garnet textures in each mount, using an FEI Quanta 200 environmental SEM and a MonoCL detector attached on a JXA-8100 electron microprobe at the State Key Laboratory of Geological Processes and Mineral Resources, China University of Geosciences, Wuhan. Major elements of the garnets were analyzed using a JEOL JXA 8230 electron probe microanalyzer equipped with wavelength and energy-dispersive detectors at the Center for Material Research and Analysis, Wuhan University of Technology. The operating conditions for the wavelength-dispersive analyses consisted of an accelerating voltage of 20 kV, a beam current of 20 nA, and a beam diameter of 5 μm. Natural silicate minerals were used as standards, including albite [Na], sanidine [K], chromite [Cr], rhodonite [Ca, Mn], hematite [Fe], pyrope [Al, Si], olivine [Mg], and rutile [Ti]. Spectral lines, peak time (seconds), off-peak background time (seconds), and average minimum detection limits (weight percent) used for the wavelength-dispersive spectroscopy analyses are as follows: K (Kα, 10, 5, 0.03), Na (Kα, 10, 5, 0.03), Cr (Kα, 10, 5, 0.04), Si (Kα, 10, 5, 0.03), Al (Kα, 10, 5, 0.025), Mg (Kα, 10, 5, 0.02), Ca (Kα, 10, 5, 0.018), Ti (Kα, 10, 5, 0.015), Mn (Kα, 10, 5, 0.04), and Fe (Kα, 20, 10, 0.035). Each spot analysis was adjacent to the ion microprobe analysis pit produced by the oxygen isotope analysis.

Oxygen Isotope Analysis by SIMS. In situ oxygen isotope analyses of all garnet grains were carried out using the WiscSIMS CAMECA IMS-1280 multicollector ion microprobe at the Department of Geoscience, University of Wisconsin–Madison in two consecutive sessions (5 d in total). Samples were chemically washed and coated with ~60 nm of high-purity gold prior to SIMS analysis. A 1.7- to 3.1-nA Cs^+ primary ion beam with a total impact energy of 20 keV was focused to a diameter of ~8 × 12 μm on the gold-coated sample surface (43–45). Secondary $^{16}O^-$, $^{16}OH^-$, and $^{18}O^-$ ions were detected simultaneously on three Faraday cup detectors. An electron gun and conductive gold coating were used to compensate for electrical charging on the sputtered surface. The intensities of $^{16}O^-$ and $^{18}O^-$ were 2.5 to 4.7 × 10^9cps and 5.0 to 9.5 × 10^6 cps, respectively. The mass resolution (M/ΔM) was set to ~4,700,

enough to separate $^{16}OH^-$ and $^{17}O^-$. The magnetic field was regulated by an NMR probe with stability of mass better than 10 μg/g per 10 h (45). Each analysis lasted about 3.5 min, including 10-s presputtering, 120 s of automated centering of secondary ions, and 80 s for data collection. Instrument stability during the analytical session was monitored by eight repeated analyses of the UWG-2 reference material used to bracket every 5 to 20 analyses in unknown samples. The uncertainty of each bracketed set of unknowns is given as the 2SD of the bracketing UWG-2 reference material. The average repeatability of UWG-2 was ± 0.30‰ (2SD) in both analytical sessions.

Instrumental bias generated by matrix effects (compositionally dependent instrumental mass fractionation) required a correction due to the different compositions between Dongping garnet and UWG-2. A suite of eight garnet reference materials (UWPp-1, R-53, GrsSE, 92LEW7, 92LEW8, Sps-3, Sps-4, and Pyr-2) with known chemical and oxygen isotope cation compositions (16, 37, 42, 46), which bracket those of the Dongping garnets in our study, were analyzed at the start of each analytical session to determine four calibration curves for Ca^{2+}, Fe^{3+}, Mn^{2+}, and Fe^{2+} cations (see details in Datasets S6 and S7 and embedded figures). Corrections for matrix effects were thus applied by using the above calibration curves with the corresponding Ca^{2+} (atoms per formula unit, a.p.f.u.), Fe^{3+} (a.p.f.u.), Mn^{2+} (a.p.f.u.), and Fe^{2+} (a.p.f.u.) of measured in Dongping garnet grains by EPMA near each SIMS pit. Detailed correction protocols follow those suggested by Page et al. (16) and Kitajima et al. (46), which result in an accuracy of ± 0.5 to 0.6‰ (2SD). Composition bias corrections for this study range from 4.7 to 8.2‰ (*SI Appendix*, Dataset S4). Oxygen isotope compositions of Dongping garnet are expressed relative to the V-SMOW scale.

Trace Element Analysis by LA-ICP-MS. Trace element analysis of garnet was conducted by LA-ICP-MS at the Wuhan Sample Solution Analytical Technology Co., Ltd., Wuhan, China. Laser sampling was performed using a GeolasPro laser ablation system that consists of a COMPexPro 102 ArF excimer laser (wavelength of 193 nm and maximum energy of 200 mJ) and a MicroLas optical system. An Agilent 7700e ICP-MS instrument was used to acquire ion-signal intensities. Helium was applied as a carrier gas. Argon was used as the make-up gas and mixed with the carrier gas via a T connector before entering the ICP. A "wire" signal smoothing device is included in this laser ablation system (47). The spot size and frequency of the laser were set to 32 μm and 6 Hz, respectively. Trace element compositions of minerals were calibrated against various reference materials (BHVO-2G, BCR-2G, and BIR-1G) without using an internal reference (48). Each analysis incorporated a background acquisition of ~20 to 30 s followed by 50 s of data acquisition from the sample. The Excel-based software program ICPMSDataCal was used to perform off-line selection and integration of background and analyzed signals, time-drift correction, and quantitative calibration for the trace element analysis (48).

Calculation of $\delta^{18}O$ Values of Garnet-Forming Aqueous Fluid. Given that Dongping garnet formed at the temperature of 383 to 302 °C (18), the fractionation equations of Zheng (20) for garnet-water were adopted to calculate the $\delta^{18}O$ values of garnet-forming aqueous fluid:

$$\Delta^{18}O_{(Phase1\ -\ Phase2)} \approx 1{,}000\ln_{1\text{–}2} = A_{1\text{–}2} \times 10^6/T^2 + B_{1\text{–}2} \times 10^3/T + C_{1\text{–}2}, \quad [1]$$

where T is the temperature in Kelvin. The coefficients are used for grossular-water fractionation (A = 3.74, B = −9.11, C = 2.52) and andradite-water fractionation (A = 3.76, B = −9.05, C = 2.52).

Fluid–Rock Interaction. Fluid–rock interaction involving oxygen isotope exchange between magmatic fluid [$\delta^{18}O_{water}$ = 10 to 5‰ (21, 22)], meteoric water [$\delta^{18}O_{water}$ = −12.5‰ (30, 31)], and the ore-hosting syenite [average $\delta^{18}O$ = 7.1‰ (30)] were modeled based on the mass balance isotopic equations of Taylor (49):

$$W\delta^{18}O_{i.\ water} + R\ \delta^{18}O_{i.\ rock} = W\ \delta^{18}O_{f.\ water} + R\ \delta^{18}O_{f.\ rock}, \quad [2]$$

where W = atom percent of the oxygen isotope in hydrothermal fluid, R = atom percent of the oxygen isotope in the rock, and $\delta^{18}O_{i.}$ and $\delta^{18}O_{f.}$ are the initial and final oxygen isotopic compositions, respectively, of the rock and fluid involved in the isotopic exchange reactions.

Thus, the water/rock ratio in atom percent (W/R) can be expressed as

$$W/R = (\delta^{18}O_{f.\ rock} - \delta^{18}O_{i.\ rock})/(\delta^{18}O_{i.\ water} - \delta^{18}O_{f.\ water}). \quad [3]$$

Combining with Eq. **4**,

$$\Delta^{18}O_{rock-water} = \delta^{18}O_{f.\ rock} - \delta^{18}O_{f.\ water}, \quad [4]$$

Eq. **3** can be rewritten as

$$\delta^{18}O_{f.\ water} = [\delta^{18}O_{i.\ rock} + (W/R) \times \delta^{18}O_{i.\ water} - \Delta^{18}O_{rock\text{–}water}]/[1 + (W/R)], \quad [5]$$

where $\Delta^{18}O_{rock\text{–}water}$ is the temperature-dependent rock–fluid relative isotopic fractionation. For granitic rocks (represented here by the syenite), $\delta^{18}O_{f.\ rock}$ is usually equal to the $\delta^{18}O$ value of plagioclase (An_{30}) (49), and thus the feldspar-water geothermometer can be used to calculate $\Delta^{18}O_{rock\text{-}water}$ at any temperature [$1{,}000\ln\alpha = 2.68 \times (10^6/T^2) - 3.29$, where the T is the temperature in Kelvin] (50).

The above W/R ratio is assumed based on continuous circulation and cyclic reequilibration of hydrothermal fluid with the host rock (49). However, some of the heated hydrothermal fluid could have been lost during fluid–rock interaction. In the extreme open-system case in which each increment of fluid makes only a single pass through the host rock, W/R can be expressed as

$$(W/R)_{open\ system} = \ln\left[(W/R)_{closed\ system} + 1\right]. \quad [6]$$

The changes in $\delta^{18}O$ values of the resultant fluid in closed and open systems are graphically shown in *SI Appendix*, Fig. S6 *A–C*.

Estimation of Meteoric Water Contribution. The fraction contribution (A) of meteoric water in the hydrothermal fluid system can be estimated based on the isotopic mass balance for a binary mixing model with end members of meteoric water ($\delta^{18}O_{meteoric\ water}$) and magmatic fluid ($\delta^{18}O_{magmatic\ fluid}$):

$$\delta^{18}O_{f.\ water} = A \times \delta^{18}O_{meteoric\ water} + (1\text{–}A) \times \delta^{18}O_{magmatic\ fluid}. \quad [7]$$

As discussed above, the average $\delta^{18}O$ value of Early Cretaceous meteoric water at Dongping is constrained at −12.5‰. The $\delta^{18}O$ value of end member of magmatic fluid at Dongping is difficult to precisely constrain due to the absence of exposed intrusions genetically related to gold genesis (18). Magmatic fluid generally has $\delta^{18}O$ values of 10 to 5‰ (21, 22), and thus a $\delta^{18}O$ value of 10‰ can be assumed to estimate the maximum A. The highest $\delta^{18}O_{water}$ value at Dongping is 6.1‰ (Fig. 3 and *SI Appendix*, Fig. S5*B*), which can be assumed to estimate the minimum A. The calculated results are reported in Dataset S5.

Data Availability. All study data are included in the article and/or supporting information.

ACKNOWLEDGMENTS. This research is financially supported by the Ministry of Science and Technology of China (Grant 2016YFC0600104), National Natural Science Foundation of China (Grant 41325007), and Fundamental Research Funds for National University, China University of Geosciences (Wuhan). We thank Noriko Kita, Mike Spicuzza, and Kouki Kitajima for their skilled assistance during oxygen isotope analysis at the WiscSIMS laboratory. WiscSIMS is supported by NSF (EAR-2004618) and the University of Wisconsin–Madison. We sincerely thank the editor-in-chief (May R. Berenbaum) and three anonymous referees who provided insightful reviews and constructive suggestions that have been very useful in improving the presentation.

Author affiliations: [a]State Key Laboratory of Geological Process and Mineral Resources, China University of Geosciences, Wuhan 430074, China; [b]School of Earth Resources, China University of Geosciences, Wuhan 430074, China; [c]WiscSIMS, Department of Geoscience, University of Wisconsin–Madison, Madison, WI 53706; [d]Deutsches GeoForschungsZentrum GFZ, Potsdam 14473, Germany; and [e]Institute of Geology and Geophysics, Chinese Academy of Sciences, Beijing 100029, China

1. H. E. Frimmel, Earth's continental crustal gold endowment. *Earth Planet. Sci. Lett.* **267**, 45–55 (2018).
2. R. J. Goldfarb *et al.*, "Distribution, character, and genesis of gold deposits in metamorphic terrains" in *Economic Geology 100th Anniversary Volume*, J. W. Hedenquist, J. F. H. Thompson, R. J. Goldfarb, J. P. Richards, Eds. (Society of Economic Geologists, Littleton, CO, 2005), pp. 407–450.
3. G. N. Phillips, R. Powell, Formation of gold deposits: A metamorphic devolatilization model. *J. Metamorph. Geol.* **28**, 689–718 (2010).
4. A. G. Tomkins, Windows of metamorphic sulfur liberation in the crust: Implications for gold deposit genesis. *Geochim. Cosmochim. Acta* **74**, 3246–3259 (2010).

5. R. J. Goldfarb, D. I. Groves, Orogenic gold: Common or evolving fluid and metal sources through time. *Lithos* **233**, 2–26 (2015).
6. D. I. Groves *et al.*, A holistic model for the origin of orogenic gold deposits and its implications for exploration. *Miner. Depos.* **54**, 1–18 (2019).
7. D. R. Burrows, P. C. Wood, E. T. C. Spooner, Carbon isotope evidence for a magmatic origin for Archean gold-quartz vein ore deposits. *Nature* **321**, 851–854 (1986).
8. A. G. Mueller *et al.*, Archaean high Mg monzodiorite syenite epidote skarn, and biotite sericite gold lodes in the Granny Smith-Wallaby district, Australia: U-Pb and ReOs chronometry of two intrusion related hydrothermal systems. *Miner. Depos.* **43**, 337–362 (2008).
9. J. W. Li *et al.*, Giant Mesozoic gold provinces related to the destruction of the North China craton. *Earth Planet. Sci. Lett.* **349–350**, 26–37 (2012).
10. Y. Xue, I. Campbell, T. R. Ireland, P. Holden, R. Armstrong, No mass-independent sulfur isotope fractionation in auriferous fluids supports a magmatic origin for Archean gold deposits. *Geology* **41**, 791–794 (2013).
11. K. M. Helt, A. E. Williams-Jones, J. R. Clark, B. A. Wing, R. P. Wares, Constraints on the genesis of the Archean oxidized, intrusion-related Canadian Malartic gold deposit, Quebec, Canada. *Econ. Geol.* **109**, 713–735 (2014).
12. T. C. McCuaig, R. Kerrich, P–T–t–deformation–fluid characteristics of lode gold deposits: Evidence from alteration systematics. *Ore Geol. Rev.* **12**, 381–453 (1998).
13. K. Neyedley, J. J. Hanley, M. Fayek, D. J. Kontak, Textural, fluid inclusion, and stable oxygen isotope constraints on vein formation and gold precipitation at the 007 deposit, Rice Lake Greenstone Belt, Bissett, Manitoba, Canada. *Econ. Geol.* **112**, 629–660 (2017).
14. M. J. Kerr *et al.*, Evidence of upgrading of gold tenor in an orogenic quartz-carbonate vein system by late magmatic-hydrothermal fluids at the Madrid Deposit, Hope Bay Greenstone Belt, Nunavut, Canada. *Geochim. Cosmochim. Acta* **241**, 180–218 (2018).
15. D. Vielzeuf, M. Veschambre, F. Brunet, Oxygen isotope heterogeneities and diffusion profile in composite metamorphic-magmatic garnets from the Pyrenees. *Am. Mineral.* **90**, 463–472 (2005).
16. F. Z. Page, N. T. Kita, J. W. Valley, Ion microprobe analysis of oxygen isotopes in garnets of complex chemistry. *Chem. Geol.* **270**, 9–19 (2010).
17. F. J. Nie, Geology and origin of the Dongping alkalic-type gold deposit, northern Hebei Province, People's Republic of China. *Resour. Geol.* **48**, 139–158 (1998).
18. G. H. Fan, J. W. Li, X. D. Deng, W. S. Gao, S. Y. Li, Age and origin of the Dongping Au-Te deposit in the North China Craton revisited: Evidence from paragenesis, geochemistry, and in situ U-Pb geochronology of garnet. *Econ. Geol.* **116**, 963–985 (2021).
19. M. Gaspar, C. Knaack, L. D. Meinert, R. Moretti, REE in skarn systems: A LA-ICP-MS study of garnets from the Crown Jewel gold deposit. *Geochim. Cosmochim. Acta* **72**, 185–205 (2008).
20. Y. F. Zheng, Calculation of oxygen isotope fractionation in anhydrous silicate minerals. *Geochim. Cosmochim. Acta* **57**, 1079–1091 (1993).
21. H. P. Taylor, The application of oxygen and hydrogen isotope studies to problems of hydrothermal alteration and ore deposition. *Econ. Geol.* **69**, 843–883 (1974).
22. A. C. Harris, S. D. Golding, New evidence of magmatic-fluid-related phyllic alteration implications for the genesis of porphyry Cu deposits. *Geol.* **30**, 335–338 (2002).
23. F. P. Bierlein, D. Crowe, Phanerozoic orogenic lode gold deposits. *Rev. Econ. Geol.* **13**, 103–139 (2000).
24. L. Mathieu, Detecting magmatic-derived fluids using pyrite chemistry: Example of the Chibougamau area, Abitibi Subprovince, Québec. *Ore Geol. Rev.* **114**, 103–127 (2019).
25. S. F. Simmons, K. L. Brown, Gold in magmatic hydrothermal solutions and the rapid formation of a giant ore deposit. *Science* **314**, 288–291 (2006).
26. J. L. Muntean, J. S. Cline, A. C. Simon, A. A. Longo, Magmatic-hydrothermal origin of Nevada's Carlin-type gold deposits. *Nat. Geosci.* **4**, 122–127 (2011).
27. M. J. Kohn, J. W. Valley, Effects of cation substitutions in garnet and pyroxene on equilibrium isotope fractionations. *J. Metamorph. Geol.* **16**, 625–639 (1998).
28. J. Horita, D. R. Cole, D. J. Wesolowski, The activity-composition relationship of oxygen and hydrogen isotopes in aqueous salt solutions: III. Vapor-liquid water equilibration of NaCl solutions to 350°C. *Geochim. Cosmochim. Acta* **59**, 1139–1151 (1995).
29. K. I. Shmulovich, D. Landwehr, K. Simon, W. Heinrich, Stable isotope fractionation between liquid and vapour in water-salt systems up to 600°C. *Chem. Geol.* **157**, 343–354 (1999).
30. Z. C. Zhang, Characteristics of H and O isotopes and fluid evolution in Dongping gold deposit. *G. Geol.* **30**, 36–41 (1996).
31. Z. J. Zha, "Geological and geochemical characteristics and genesis of the Zhongshangou gold deposit in northwest Hebei Province," M.S. thesis, China University of Geosciences, Beijing (2020), pp. 54–56.
32. H. Craig, Isotopic variations in meteoric water. *Science* **133**, 1702–1703 (1961).
33. D. E. Crowe, L. R. Riciputi, S. Bezenek, A. Ignatiev, Oxygen isotope and trace element zoning in hydrothermal garnets: Windows into large-scale fluid-flow behavior. *Geology* **29**, 479–482 (2001).
34. C. C. Clechenko, J. W. Valley, Oscillatory zoning in garnet from the Willsboro Wollastonite Skarn, Adirondack Mts, New York: A record of shallow hydrothermal processes preserved in a granulite facies terrane. *J. Metamorph. Geol.* **21**, 771–784 (2003).
35. J. Ryan-Davis *et al.*, Andradite skarn garnet records of exceptionally low δ 18 O values within an Early Cretaceous hydrothermal system, Sierra Nevada, CA. *Contrib. Mineral. Petrol.* **174**, 1–19 (2019).
36. C. Chelle-Michou, B. Rottier, L. Caricchi, G. Simpson, Tempo of magma degassing and the genesis of porphyry copper deposits. *Sci. Rep.* **7**, 40566 (2017).
37. S. E. Gelman, F. J. Gutiérrez, O. Bachmann, On the longevity of large upper crustal silicic magma reservoirs. *Geology* **41**, 759–762 (2013).
38. A. E. Williams-Jones, R. J. Bowell, A. A. Migdisov, Gold in solution. *Elements* **5**, 281–287 (2009).
39. G. S. Pokrovski, N. N. Akinfiev, A. Y. Borisova, A. V. Zotov, K. Kouzmanov, Gold speciation and transport in geological fluids: Insights from experiments and physical-chemical modelling. *Geol. Soc. Lond. Spec. Publ.* **402**, 9–70 (2014).
40. Z. W. Bao, C. J. Li, Z. H. Zhao, Metallogeny of the syenite-related Dongping gold deposit in the northern part of the North China Craton: A review and synthesis. *Ore Geol. Rev.* **73**, 198–210 (2016).
41. J. J. Wilkinson, J. D. Johnston, Pressure fluctuations, phase separation, and gold precipitation during seismic fracture propagation. *Geology* **24**, 395–398 (1996).
42. J. W. Valley, N. Kitchen, M. J. Kohn, C. R. Niendorf, M. J. Spicuzza, UWG-2, a garnet standard for oxygen isotope ratios: Strategies for high precision and accuracy with laser heating. *Geochim. Cosmochim. Acta* **59**, 5223–5231 (1995).
43. J. W. Valley, N. T. Kita, "In situ oxygen isotope geochemistry by ion microprobe" in *Secondary Ion Mass Spectrometry in the Earth Sciences*, M. Fayek, Ed. (Mineralogical Association of Canada, 2009), vol. **41**, pp. 19–63.
44. N. T. Kita, T. Ushikubo, B. Fu, J. W. Valley, High precision SIMS oxygen isotope analyses and the effect of sample topography. *Chem. Geol.* **264**, 1–4 (2009).
45. N. T. Kita, J. M. Huberty, R. Kozdon, B. L. Beard, J. W. Valley, High-precision SIMS oxygen, sulfur and iron stable isotope analyses of geological materials: Accuracy, surface topography and crystal orientation. *Surf. Interface Anal.* **43**, 427–431 (2011).
46. K. Kitajima, A. Strickland, M. J. Spicuzza, T. J. Tenner, J.W. Valley, Improved matrix correction of δ18O analysis by SIMS for pyralspite and Cr-pyrope garnets. *Goldschmidt Abstracts* **2016**, 1542 (2016).
47. Z. C. Hu *et al.*, "Wave" signal-smoothing and mercury-removing device for laser ablation quadrupole and multiple collector ICPMS analysis: Application to lead isotope analysis. *Anal. Chem.* **87**, 1152–1157 (2015).
48. Y. S. Liu *et al.*, In situ analysis of major and trace elements of anhydrous minerals by LA-ICP-MS without applying an internal standard. *Chem. Geol.* **257**, 34–43 (2008).
49. H. P. Taylor, Water/rock interactions and the origin of H_2O in granitic batholiths. *J. Geol. Soc. London* **133**, 509–558 (1977).
50. E. Taylor, Magmatic volatiles; isotopic variation of C, H, and S. *Rev. Mineral.* **16**, 185–225 (1986).